Agglomerated polymer monoliths with bimetallic nano-particles as flow-through micro-reactors

ARTICLE *in* MICROCHIMICA ACTA · JULY 2012

Impact Factor: 3.74 · DOI: 10.1007/s00604-012-0865-7

5 AUTHORS, INCLUDING:

Patrick Gerard Floris
Dublin City University
7 PUBLICATIONS **295** CITATIONS
SEE PROFILE

Pavel N Nesterenko
University of Tasmania
262 PUBLICATIONS **2,876** CITATIONS
SEE PROFILE

Brett Paull
University of Tasmania
240 PUBLICATIONS **3,048** CITATIONS
SEE PROFILE

Damian Connolly
Waterford Institute of Technology
53 PUBLICATIONS **674** CITATIONS
SEE PROFILE

Microchim Acta (2012) 179:149–156
DOI 10.1007/s00604-012-0865-7

ORIGINAL PAPER

Agglomerated polymer monoliths with bimetallic nano-particles as flow-through micro-reactors

Patrick Floris · Brendan Twamley · Pavel N. Nesterenko · Brett Paull · Damian Connolly

Received: 26 April 2012 / Accepted: 9 July 2012 / Published online: 22 August 2012

Abstract Polymer monoliths in capillary format have been prepared as solid supports for the immobilisation of platinum/palladium bimetallic nano-flowers. Optimum surface coverage of nano-flowers was realised by photografting the monoliths with vinyl azlactone followed by amination with ethylenediamine prior to nano-particle immobilisation. Field emission SEM imaging was used as a characterisation tool for evaluating nano-particle coverage, together with BET surface area analysis to probe the effect of nano-particle immobilisation upon monolith morphology. Ion exchange chromatography was also used to confirm the nature of the covalent attachment of nano-flowers on the monolithic surface. In addition, EDX and ICP analyses were used to quantify platinum and palladium on modified polymer monoliths. Finally the catalytic properties of immobilised bimetallic Pd/Pt nano-flowers were evaluated in flow-through mode, exploiting the porous interconnected flow-paths present in the prepared monoliths (pore diameter~1–2 μm). Specifically, the reduction of Fe (III) to Fe (II) and the oxidation of NADH to NAD^+ were selected as model redox reactions. The use of a porous polymer monolith as an immobilisation substrate (rather than aminated micro-spheres) eliminated the need for a centrifugation step after the reaction.

Keywords Nano-particles · Agglomerated monolith · Micro-reactor · Flow-through catalysis

Introduction

Micro-reactors have gained the attention of researchers over the last decade for their ability to process traditional chemical reactions using much smaller volumes, hence proving to be simultaneously more economical and environmentally sustainable.

Metal nano-particles (NPs) have been widely used in micro-reactors [1, 2] due to their higher surface to volume ratio. The ability to generate nano-structures of various morphologies is of fundamental importance in order to fully exploit the catalytic capabilities of such materials. Branched shaped nano-particles have proven to be particularly interesting [3–5] as their surface roughness and tendency to exhibit highly active facets makes them attractive materials for catalysis [6]. Several synthetic routes have been developed over recent years to generate highly branched nano-structures, including kinetic controlled overgrowth, aggregation based growth, heterogeneous seeded growth, selective etching and template-directed methods [7]. Because of the need to relate catalytic activity and particle structure, bimetallic nano-materials have gained in popularity, since these types of materials can increase catalytic activity and offer alternative selectivity relative to their monometallic counterparts [8–10]. Metallic nano-materials are used either in a colloidal form or attached onto a solid support, the latter having several advantages, such as easy recovery of the

Electronic supplementary material The online version of this article (doi:10.1007/s00604-012-0865-7) contains supplementary material, which is available to authorized users.

P. Floris · D. Connolly (✉)
Irish Separation Science Cluster, National Centre for Sensor Research, Dublin City University,
Dubin 9, Ireland
e-mail: damian.connolly@dcu.ie

B. Twamley · D. Connolly
School of Chemical Sciences, Dublin City University,
Dublin 9, Ireland

P. N. Nesterenko · B. Paull
Australian Centre for Research on Separation Science (ACROSS),
School of Chemistry, University of Tasmania,
Hobart 7005, Australia

catalyst by filtration in an industrial application. The most commonly used support materials are various organic polymers [11], silica [12], carbonaceous materials [13] and metal oxides [14].

Among the various support options, monolithic porous supports have gained importance over the recent years [15]. Organo polymer monoliths exhibit several advantages as support phases, as they can be readily generated in various moulds in situ, and by controlling the monomer to porogen ratio, pores of desired size can be obtained. These properties make polymer monoliths attractive for flow-through catalytic applications, as firstly the necessity of a filtration/centrifugation step required in heterogeneous catalysis is removed, and secondly they can be easily incorporated into micro-reactors (without the need of retaining frits). A few catalytic applications of NPs immobilised on monolithic supports are documented in the literature [15]. Generally metal NPs can be immobilised by in situ reduction from metal ions or by pumping a colloid through a monolith modified with either amino, cyano or thiol functional groups [16]. However, there are very few reports describing catalytic applications using monoliths as supports in flow-through mode. Nikbin et al. [17] described the synthesis of a styrenic monolith bearing quaternary amine groups through which a solution of palladium salt was flushed through followed by reducing to Pd^0 by using $NaBH_4$. Heck coupling reactions were performed with high yields but a serious drawback was represented by the heavy leaching of Pd into the product which required the use of a second column for Pd trapping. Alternatively, Bandari et al. [18] described the preparation of a polymethacrylate based monolith via electron beam polymerisation, within the confinements of a 2 cm×30 cm stainless steel column. The surface was functionalised with N,N-dipyrid-2-ylmethacryl amide groups and Pd NPs, synthesised in situ from Pd^{2+} ions, and was successively used for Heck coupling reactions under a continuous flow procedure, with only a limited leaching of Pd observed at 4.2 %. Also Mennecke et al. [19] reported the use of an aminated co-polymer of DVB, styrene and vinylbenzyl chloride inside glass as a surface to immobilise Pd NPs by a process of ion exchange. These functionalised Raschig-rings where placed inside a housing with a dead-volume of 1–2 mL and Suzuki-Miyaura coupling reactions were performed in a cyclic mode, since single pass experiments did not result in any product yield. Other flow-through catalytic applications involving monoliths in capillary format have been reported, however in these examples the monoliths have not been functionalised with metal NPs, but metal-ligand complexes instead [20–22].

In the present paper the application of agglomerated polymer monoliths with bimetallic nano-particles as flow-through micro-reactors is reported. To the authors knowledge this represents the first investigation into the immobilisation of Pd/Pt nano-flowers on a variety of organo-polymer monoliths in capillary format, and their subsequent application as flow-through catalytic reactors for selected redox reactions.

Experimental

Materials and reagents

Benzophenone, 2,2-dimethoxy-2-phenylacetophenone (DAP), glycidyl methacrylate (GMA), ethylene glycol dimethacrylate (EDMA), butyl methacrylate (BUMA), 1-decanol, ethylenediamine, poly(vinyl pyrrolidone) (PVP), ascorbic acid, citric acid, sodium tetrachloropalladate, potassium tetrachloroplatinate, nitric acid and hydrochloric acid were all purchased from Sigma-Aldrich (Dublin, Ireland, www.sigmaaldrich.com). 4,4-Dimethyl-2-vinyl-2-oxazolin-5-one (VAL) was purchased from TCI Europe (Zwijndrecht, Belgium, www.tcichemicals.com/en/eu). Methanol, ethanol, acetone and acetonitrile were of HPLC grade and purchased from Fisher Scientific (Dublin, Ireland, www.ie.fishersci.com). All chemicals were used as received and without further purification. Teflon-coated fused silica capillary (100 μm i.d.) was supplied by Composite Metal Services (Shipley, England, www.cmscientific.com).

Instrumentation

Photo-polymerisation and photo-grafting were carried out using a Spectrolinker XL-1000 UV Crosslinker at 254 nm (Spectronics Corp., Westbury, NY, USA, www.spectroline.com). The balance used was a Sartorius Extend (Sartorius, Goettingen, Germany, www.sartorius.com). A KD Scientific syringe pump (KDS-100-CE, KD Scientific Inc, Holliston, MA, USA, www.kdscientific.com) was used for all washing and functionalisation of monoliths, while a Model K120 Knauer pump (Knauer, Berlin, Germany, www.knauer.net) was used for the immobilisation of nano-particles and evaluating the effect of contact time on the catalytic activity of immobilised nano-particles. Field emission scanning electron microscopy (SEM) was performed using a Hitachi S-5500 instrument (Hitachi, Maidenhead, UK) equipped with an Oxford Instruments PentaFETx3 detector with the INCA Microanalysis Suite (Oxford Instruments, Oxfordshire, UK). UV spectra were obtained using a Lambda 900 UV–vis spectrophotometer (Perkin Elmer, USA, www.perkinelmer.com), while for measurements in flow-through mode a UV spectrometer with a 3 nL flow cell was used (Dionex Ultimate LC system, Sunnyvale, CA, USA, www.dionex.com). A Varian ICP-AES was used for determination of metal concentrations in nano-agglomerated CIM disk monoliths. A capillary ICS-

5000 system (Dionex, Sunnyvale, CA, USA, www.dionex.com) was used for the characterisation of ion-exchange properties of nano-agglomerated monoliths.

Preparation of Pd/Pt nano-flowers

Pd/Pt nano-flowers were prepared as described elsewhere [23] and involves the overgrowth of platinum "petals" upon a palladium core nano-crystal. The exact procedure is presented in Electronic Supplementary Material (ESM).

Preparation of polymer monoliths

A series of monoliths were fabricated by preparing various monomer/porogen mixtures as described in Table 1. Monolith GMA-1 incorporated encapsulated nano-flowers which were admixed into the monomer mixture prior to polymerisation. All other monoliths were aminated after polymerisation prior to flushing nano-flowers across the monolith. Monoliths BuMA-1 and BuMA-2 were photografted with GMA and vinyl azlactone respectively prior to amination in order to maximise the coverage of nano-flowers. Detailed protocols are provided in ESM.

Amination of disk monoliths

GMA-co-EDMA disks (Convective Interactive Media (CIM) Discs) with epoxy functionality were kindly donated by Bia Separations (Slovenia). These were flushed for 6 h at room temperature with 1 M ethylenediamine to functionalise the surface with free NH_2 functional groups and they were finally rinsed with water.

Immobilisation of nano-flowers

A 1 in 10 dilution of nano-flowers was pumped across the monoliths which turned gradually black during the coating step as described in ESM. The concentration of metals present on a CIM disk sample was determined by ICP-AES. The modified monolith was placed in *aqua regia* to allow dissolution of the metals. Prior to analysis, this sample was diluted 1 in 50 for Pt and 1 in 9 for Pd analysis with 0.1 M HNO_3.

Catalytic reduction of Fe (III) to Fe (II) via flow-through monolithic micro-reactors

Standard redox chemistry was used to evaluate the catalytic properties of the immobilised Pd/Pt nano-flowers. A mixture of $K_3[Fe(CN)_6]$ (8 m*M*) and $NaBH_4$ (0.6 m*M*) was prepared in a pH 11.5 aqueous solution, adjusting the ionic strength to 0.085 M with NaCl. This reaction was performed using a monolith in a capillary format with immobilised Pd/Pt nano-flowers (monolith BUMA-2) at different flow-rates (10, 15 and 20 $\mu L.min^{-1}$) followed by UV–vis analysis of collected fractions. UV–vis analysis of the collected product was used to confirm the complete reduction of ferrocyanide (III) due to the elimination of the absorbance peak at 420 nm.

Results and discussion

Encapsulation of nano-flowers in polymer monoliths

The attachment of metallic nano-particles upon aminated surfaces has been reported before [24, 25], however an optimal methodology for controlling the level of coverage of such materials is not clearly described in the literature. In this paper various types of monoliths were prepared, which were then used to evaluate the impact of several parameters upon the final level of coverage. These included the effect of encapsulation of nano-particles into the monomer mixture, the effects of varying the amount of epoxy groups on the monolith's surface, and the impact of grafting amine-reactive polymer chains onto the surface of a pre-formed monolith. Synthetic parameters known to affect monolith morphology (pore size and surface area) such as porogen composition [26] and polymerisation conditions were held constant; therefore variations in the nano-particle coverage

Table 1 Summary of polymer monoliths prepared for modification with metal nano-materials

Monolith[a]	GMA (wt%)	BUMA (wt%)	EDMA (wt %)	Decanol (wt%)	Propanol (wt%)	1,4-Butanediol (wt %)	H_2O[b] (wt%)	Grafted GMA (wt%)	Grafted VAL (wt%)
GMA-1	22.5	–	7.5	–	35	28	7	–	–
GMA-2 %	2	22	16	60	–	–	–	–	–
GMA-6 %	6	18	16	60	–	–	–	–	–
GMA-12 %	12	12	16	60	–	–	–	–	–
GMA-24 %	24	0	16	6	–	–	–	–	–
BUMA-1	–	24	16	60	–	–	–	15	–
BUMA-2	–	24	16	60	–	–	–	–	–

[a]All monoliths contained DAP as initiator, 1 % w.r.t. monomer

[b]Aqueous suspension of Pd/Pt nano-flowers

ultimately observed could attributed to tailored monolith surface chemistry. In a first step, flower shaped nano-materials consisting of a palladium core and platinum branches of approximately 20 nm in size were synthesised according to the procedure described by Lim et al. [23]. The dendritic nano-architecture of the resulting particles, which in previous reports has been likened to snowflake-like or flower-like structures, can be clearly seen in Fig. 1(a). An obvious strategy to incorporate nano-materials in a polymer monolith is to embed or "encapsulate" them within the bulk polymer globules during polymerisation, as has been reported previously by Thabano et al. [27] and more recently by Krenkova et al. [28]. Typically the monomer mixture is designed in such a way that the nano-particles form a stable suspension prior to polymerisation and their concentration can be controlled across a reasonably broad range. However, the independent control of monolith morphology and nano-particle loading is difficult to achieve using this approach. In the initial stages of the work presented herein, a monomer mixture was prepared, which was gray in colour but transparent, which was a good indicator of colloidal stability prior to UV initiated polymerisation. However, field emission scanning electron microscopy images of a cross-section of the resulting monolith (GMA-1 shown in Fig. 1b) shows that no nano-particles were presented at the monolith surface (which would appear as white dots). Further attempts to increase the nano-particle concentration in monomer mixtures lead to either cloudy monomer mixtures, or gross precipitation of aggregated nano-particles. Although the porogen composition could have been optimised to include more water (1-propanol/1,4-butanediol/water), this strategy was also not pursued since higher levels of water in this well-studied ternary porogen mixture is known to result in unfavourable monolith morphology [29]. Hence, all further optimisation of nano-particle coverage involved tailored control of the monolith surface chemistry based

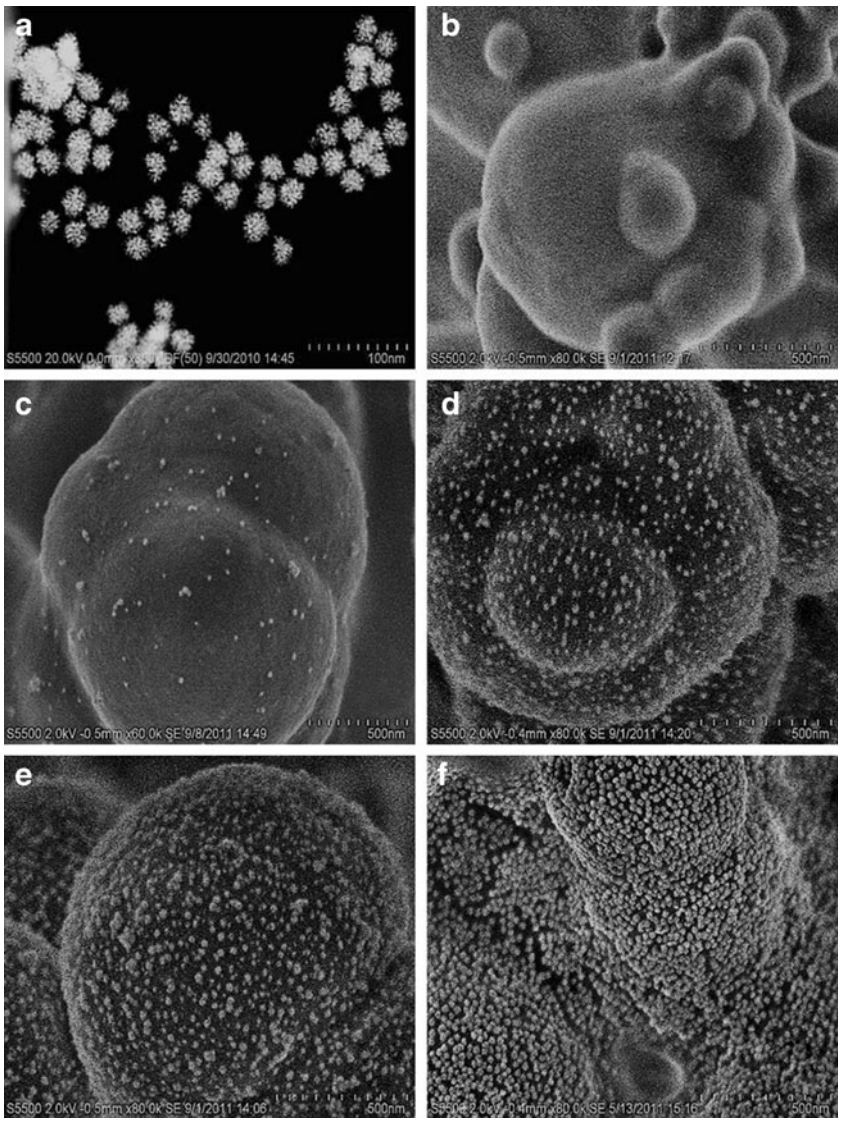

Fig. 1 FE-SEM images of (**a**) Pd/Pt nano-flowers (magnification 300,000x), (**b**) monolith GMA-1 (magnification 80,000x), (**c**) monolith GMA-2 % (magnification 60,000x), (**d**) monolith GMA-6 % (magnification 80,000x), (**e**) monolith GMA-12 % (magnification 80,000x) and (**f**) monolith BUMA-2 (magnification 80,000x)

upon the known affinity of platinum nanoparticles for aminated surfaces [30] as described in the following sections.

Modification of monolith surface chemistry via co-polymerisation

The epoxy groups present in GMA are well known for their ability to react with amino moieties [16], so ethylenediamine was reacted with a number of BuMA-*co*-GMA-*co*-EDMA monoliths, in which the concentration of GMA was varied systematically from 2 % to 24 %, while holding the total functional monomer concentration (BuMA+GMA) and the total crosslinker concentration (EDMA) constant, as shown in Table 1. The controlled increase in the distribution of amine-reactive epoxy groups presented at the monolith surface can be indirectly visualised by inspection of the relative coverage of nano-flowers in Fig. 1 (c,d,e). Relatively sparse nano-flower coverage was obtained with the GMA-2 % monolith (19 nano-flowers/500 nm^2) whereas a considerable increase in coverage is obtained for the GMA-6 % monolith (98 nano-flowers/500 nm^2). Coverage was found to plateau between monoliths GMA-12 % (135 nano-flowers/500 nm^2) and GMA-24 % (data not shown). Preliminary EDX quantified spot analysis of these monoliths roughly corresponds to the visual image shown in Fig. 1—there is a rise in the amount in wt% of Pd; Pt going from a mean of 0.03; 1.1 in the GMA-2 % monolith to 1.3; 39.58 in the GMA-24 % monolith (see supporting information). Although nano-flower coverage was reasonably dense and homogeneous on monoliths incorporating ≥12 % GMA in the copolymer (Fig. 1e), nevertheless large gaps are evident on the monolith surface between adjacent nano-particles. Clearly the use of copolymerisation techniques is rather limiting in that not all amine-reactive epoxy groups will be presented at the monolith surface as documented by Hilder et al. [31]. In addition, to obtain monoliths with the desired porosity to maintain low backpressure under flowing conditions, the maximum concentration of GMA present in monoliths had to be limited in this study to 24 %. Furthermore, it is known that unwanted changes in the physical morphology (average pore size and surface area) of polymer monoliths can also occur due to relatively small variation in monomer ratios. This effect was indeed observed, with an increase in operating backpressure from 6 $bar.cm^{-1}$ for GMA-2 % to 49 $bar.cm^{-1}$ for GMA-24 % at a nominal flow rate of 5 $\mu L.min^{-1}$. Obviously the control of monolith morphology and monolith surface chemistry cannot easily be independently controlled.

Surface area measurements

A brief study of surface area effects for aminated GMA-*co*-EDMA monoliths modified with nano-flowers was carried out. Immobilisation of nano-flowers resulted in an unexpected 71 % decrease in surface area, with each nano-flower possibly causing partial blockage of mesopores as described in more detail in ESM. Nevertheless, nano-flowers were still presented directly at the surface of the monolith and sufficiently strongly attached to be used as immobilised catalysts as shall be shown later.

Modification of monolith surface chemistry via photografting

The use of photografting methods [32–34] to increase the number of nano-flower attachment sites on the monolith surface relative to the earlier described copolymerised monoliths was investigated. Initial grafting efforts involved the grafting of GMA to a BuMA-*co*-EDMA monolith (BuMA-1; Table 1). Although the graft density can be increased by control of both the incident UV energy [35] and the grafting monomer concentration [36], a relatively low concentration of 15 % GMA was chosen to minimise the possibility of UV self-screening effects. When GMA was grafted on monolith BUMA-1 followed by amination and modification with nano-flowers, there was no observed visible increase in nano-flower coverage relative to the un-grafted GMA-24 % monolith shown in Fig. 1e. Rather than exhaustively optimise GMA graft density on the monoliths, another amine-reactive monomer, vinyl azlactone (VAL) was selected as an alternative grafting monomer for monolith BuMA-2. In previously published related studies, our research group have reported excellent coverage of metallic nano-particles on monoliths grafted with VAL. This dense coverage may be due in part to higher grafting efficiency of VAL relative to GMA, an observation previously reported by Yang et al. [33]. An additional reason for more amine groups (post-modification with ethylenediamine) may be because VAL and amines react under mild conditions (room temperature) relative to GMA, which requires elevated temperatures, possibly leading to lower reaction yields. The results obtained with the VAL-grafted monolith BuMA-2 are shown in Fig. 1(f). The coverage density was increased and uniform coverage of nano-flowers was observed.

Investigation of nano-flower attachment mechanism via ion exchange chromatography

The use of monolith BuMA-2 as an ion-exchanger before and after attachment of nano-flowers confirmed that the nano-flowers were immobilised via their interaction with the surface amine groups on the monolith as discussed in detail in ESM.

Catalytic reduction of Fe (III) to Fe (II) via flow-through monolithic micro-reactors

In order to confirm that Pd/Pt nano-flowers immobilised upon a polymer monolith retain their catalytic activity, the

well known reduction of Fe (III) to Fe (II) was selected for demonstrative purposes. The strong reducing agent sodium borohydride was used as shown in the reaction scheme below, with the pH of the system adjusted to 11.5 to prevent decomposition of borohydride [37].

$$BH_4^- + 8Fe(CN)_6^{3-} + 3H_2O \rightarrow H_2BO_3^- + 8Fe(CN)_6^{4-} + 8H^+$$

The role of the reducing agent is to act as a reservoir of electrons which are donated to the immobilized nano-catalyst and are "stored" on its surface as demonstrated by Henglein et al. [38, 39]. As the ferrocyanate(III) complex comes in contact with the nano-catalyst, the electrons present are readily available to convert $8Fe(CN)_6^{3-}$ to $8Fe(CN)_6^{4-}$. The reaction between ferrocyanate and borohydride ions in the absence of a catalyst has been reported to have a half life of 5,000 s [40], while in the presence of a catalytically active material this value drastically decreases to less than 10 s. The reaction progress could be readily studied before and after passage through the nano-flower-modified reactor since the starting material ferrocyanate (III) absorbs strongly at 420 nm, whereas the ferrocyanate (II) product is colourless. As shown in Fig. 2, UV spectrum (a) was collected immediately after preparation of the ferrocyanate (III) and borohydride solution, but before passage through the micro-reactor. UV spectrum (b) was collected at a nominal time of 60 min later, showing that some modest conversion to ferrocyanate (II) has occurred in the absence of catalyst. In contrast, UV spectra (c,d,e) were collected without delay after the reaction mixture had been pumped through the micro-reactor at flow rates ranging from 10 μL.min^{-1} to 20 μL.min^{-1}. In all cases, complete reduction has occurred despite the extremely short contact time through the micro-reactor. At a volumetric flow rate of 20 μL.min^{-1} the linear velocity was 50 mm.sec^{-1} such that the contact time through a 100 mm micro-reactor was approximately 2 s.

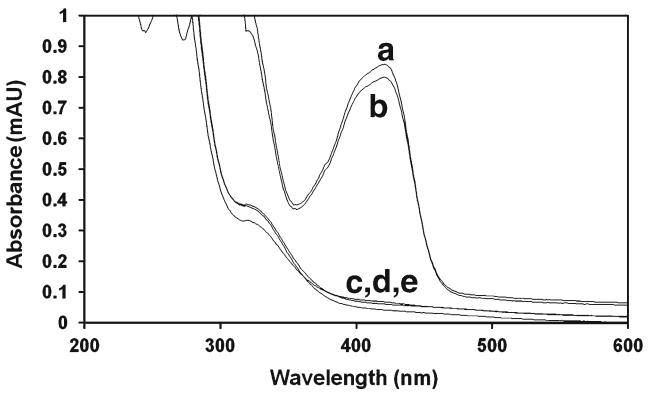

Fig. 2 UV spectra showing the reduction of (**a**) a ferrocyanate (III) solution with $NaBH_4$, (**b**) same solution after 60 min and (**c**, **d**, **e**) the original solution reduced after being pumped through the Pd/Pt modified micro-reactor

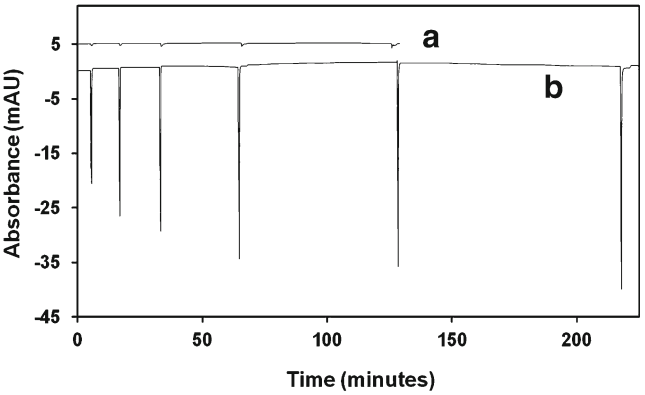

Fig. 3 UV profile at 340 nm of a 0.5 m*M* NADH solution pumped through (**a**) a blank BUMA-2 monolith, (**b**) a BUMA-2 monolith modified with Pd/Pt nano-flowers demonstrating the effects of contact time on the catalytic reaction. The flow was stopped for progressively longer time periods such as 5, 10, 15, 30, 60, 90 min and the height of the negative peak observed was proportional to the amount of NAD^+ formed

Catalytic oxidation of NADH to NAD^+ via flow-through monolithic micro-reactors

An alternative redox reaction (oxidation of NADH to NAD^+) was carried out using the micro-reactor in a "stopped flow" configuration in order to control contact time. As before, UV–vis spectroscopy was used to monitor the reaction progress. Details regarding interpretation of UV spectra for NADH/NAD^+ and the redox mechanism are provided in ESM. In the present work, aqueous NADH solutions were pumped through monolith BUMA-2 to ensure that the entire pore volume was filled. The UV detector (equipped with a 3 nL flow-cell) connected in series monitored the high absorbance of NADH at 340 nm. The flow was then interrupted and the reaction allowed to proceed

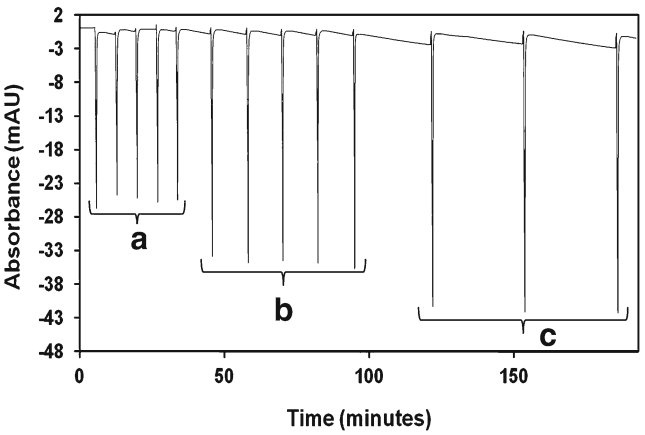

Fig. 4 Plot demonstrating the repeatability of the catalytic oxidation of NADH. Experiments were carried out using a 0.5 m*M* NADH solution by performing (**a**) 5 replicates with a 5 min contact time, (**b**) 5 replicates with a 10 min contact time, (**c**) 3 replicates with a 30 min contact time

within the micro-reactor for controlled periods of time. Turning the external pump back on then allowed the reaction product (NAD^+) to be pumped out of the reactor resulting in a negative peak due to the low extinction coefficient of NAD^+ at 340 nm.

Figure 3(b) illustrates the effect of contact time (ranging from 5 min to 90 min) on the magnitude of the negative peak. The production of NAD^+ appears to plateau after a contact time of 30 min. To demonstrate that the negative peak was due to the catalytic activity of the nano-flowers, similar experiments were performed using a blank BUMA-2 (that is, an aminated monolith not bearing immobilised nano-flowers). The baseline disturbances in Fig. 3(a) align with those in Fig. 3(b) but do not increase with time. These disturbances are due to flow disruption in the UV flow cell when the flow-rate is re-established. The effect of NADH concentration upon contact time was examined over the range 0.1 m*M* to 0.5 m*M* NADH. Figure S2 (ESM) illustrates that higher concentrations of NADH required longer contact times in order to achieve a more complete oxidation. Repeatability studies were also carried out, as shown in Fig. 4, by measuring the peak heights for replicate catalytic conversions at different contact times. The poorest % RSD (3.2 %) was for 5 min contact time, and the best was 1.1 % for 30 min (1.9 % for 10 min). Presumably poorer precision was achieved at the shorter contact time due to the reaction not having gone to completion within the micro-reactor.

Conclusion

Bimetallic nano-flowers consisting of platinum branches grown upon a palladium core have been successfully immobilised covalently on methacrylate monoliths availing of their affinity for amine functionalities. FE-SEM was used to verify that a highly dense coverage was obtained when branches of vinyl were grafted onto the monolith's surface. These monoliths were used to carry out catalytic redox reactions availing of the catalytic properties of the nano-flowers and the ideal flow-through properties of the monolithic structure. A final confirmation of the almost complete coverage of nano-flowers was assessed by using the monoliths prepared with amine functionality as weak anion exchangers. The almost complete filling of amine sites was demonstrated by the lack of retention of perchlorate which was retained when using an identically prepared monolith which only differentiated in the absence of nano-flowers.

Acknowledgments The authors would like to thank Science Foundation Ireland (Grant number 08/SRC/B1412) for research funding under the Strategic Research Cluster programme and also for equipment funding (Grant. Number 03/IN.3/1361/EC07). Also special thanks to Dr. Dario Arrua for the assistance with BET analysis and UTAS for the use of the instrumentation.

References

1. Basheer C, Hussain FSJ, Lee K, Valiyaveettil S (2004) Design of a capillary-microreactor for efficient Suzuki coupling reactions. Tetrahedron Lett 45(39):7297–7300
2. Ahmed-Omer B, Brandt JC, Wirth T (2007) Advanced organic synthesis using microreactor technology. Org Biomol Chem 5 (5):733–740
3. Grzelczak M, Perez-Juste J, Mulvaney P, Liz-Marzan LM (2008) Shape control in gold nanoparticle synthesis. Chem Soc Rev 37 (9):1783–1791
4. Xia Y, Xiong Y, Lim B, Skrabalak SE (2009) Shape controlled synthesis of metal nanocrystals: simple chemistry meets complex physics? Angew Chem Int Ed 48(1):60–103
5. Xuezhong G, Yun Y, Lijie Z, Chao Z, Ping C et al (2010) Controlled synthesis of Pt nanoparticles via seeding growth and their shaped-dependent catalytic activity. J Colloid Interface Sci 352(2):379–385
6. Jingpeng W, Dan FT, Aicheng C (2008) Direct growth of novel alloyed PtAu nanodendrites. Chem Commun 40:5010–5012
7. Byungkwon L, Younan X (2011) Metal nanocrystals with highly branched morphologies. Angew Chem Int Ed 50(1):76–85
8. Peng X, Pan Q, Rempel GL (2008) Bimetallic dendrimer-encapsulated nanoparticles as catalysts: a review of the research advances. Chem Soc Rev 37(8):1619–1628
9. Toshima N, Yonexawa T (1998) Bimetallic nanoparticles—novel materials for chemical and physical applications. New J Chem 22 (11):1179–1201
10. Chung YM, Rhee HK (2003) Partial hydrogenation of 1, 3-cyclooctadiene using dendrimer-encapsulated Pd-Rh bimetallic nanoparticles. Journal of molecular catalysis A, Chemical 206(1–2):291–298
11. Burguete IM, Garcia-Verdugo E, Luis SV, Restrepo JA (2011) Preparation of polymer-supported gold nanoparticles based on resins containing ionic liquid-like fragments: easy control of size and stability. Phys Chem Chem Phys 13(33):14831–14838
12. Budnyk P, Damin A, Agostini G, Zecchina A (2010) Gold nanoparticle aggregates immobilized on high surface area silica substrate for efficient and clean SERS applications. J Phys Chem C 114(9):3857–3862
13. Reetz MT, Winter M, Tesche B (1997) Self-assembly of tetraalkylammonium salt-stabilized giant palladium clusters on surfaces. Chem Commun 2:147–148
14. Zheng N, Stuck GD (2006) A general synthetic strategy for oxide-supported metal nanoparticle catalysts. J Am Chem Soc 128 (44):14278–14280
15. Sachse A, Galarneau A, Coq B, Fajula F (2011) Monolithic flow microreactors improve fine chemicals synthesis. New J Chem 35 (2):259–264
16. Cao Q, Xu Y, Liu F, Svec F, Fréchet JMJ (2010) Polymer monoliths with exchangeable chemistries: use of gold nanoparticles as intermediate ligands for capillary columns with varying surface functionalities. Anal Chem 82(17):7416–7421
17. Nikbin N, Ladlow M, Ley SV (2007) Continuous flow ligand-free Heck reactions using monolithic Pd [0] nanoparticles. Org Process Res Dev 11(3):458–462
18. Bandari R, Knolle W, Prager-Duschke A, Glasel HR, Buchmeiser MR (2007) Monolithic media prepared via electron beam curing for proteins separation and flow-through catalysis. Macromol Chem Phys 208(13):1428–1436
19. Mennecke K, Kirschning A (2009) Polyionic polymers—heterogeneous media for metal nanoparticles as catalyst in Suzuki-Miyaura and Heck-Mizoroki reactions under flow conditions. Beilstein J Org Chem 5:21
20. Bolton KF, Canty AJ, Deverell JA, Guijt RM, Hilder EF et al (2006) Macroporous monolith supports for continuous flow capillary microreactors. Tetrahedron Lett 47(52):9321–9324

21. Jones RC, Canty AJ, Deverell JA, Gardiner MG, Guijt RM et al (2009) Supported palladium catalysis using a heteroleptic 2-methylthiomethylpyridine-N, S-donor motif for Mizoroki-Heck and Suzuki-Miyaura coupling, including continuous organic monolith in capillary microscale flow-through mode. Tetrahedron 65(36):7474–7481
22. Gomann A, Deverell JA, Munting KF, Jones RC, Rodemann T et al (2009) Palladium-mediated organic synthesis using porous polymer monolith formed in situ as a continuous catalyst support structure for application in microfluidic devices. Tetrahedron 65 (7):1450–1454
23. Lim B, Jiang MJ, Camargo PHC, Cho EC, Tao J (2009) Pd-Pt bimetallic nanodendrites with high activity for oxygen reduction. Science 324(5932):1302–1305
24. Connolly D, Twamley B, Paull B (2010) High-capacity gold nanoparticle functionalised polymer monoliths. Chem Commun 46 (12):2109–2111
25. Grabar KC, Freeman RG, Hommer MB, Natan MJ (1995) Preparation and characterization of Au colloid monolayers. Anal Chem 67(4):735–743
26. Svec F, Fréchet JMJ (1996) New designs of macroporous polymers and supports: from separation to biocatalysis. Science 273 (5272):205–2011
27. Thabano J, Breadmore M, Hutchinson J, Johns C, Haddad PR (2009) Silica nanoparticle-templated methacrylic acid monoliths for in-line solid-phase extraction-capillary electrophoresis of basic analytes. J Chromatogr A 1216(25):4933–4940
28. Krenkova J, Lacher NA, Svec F, Fréchet JMJ (2010) Control of selectivity via nanochemistry: monolithic capillary column containing hydroxyapatite nanoparticles for separation of proteins and enrichment of phosphopeptides. Anal Chem 82(19):8335–8341
29. Peters EC, Petro M, Svec F, Fréchet JMJ (1997) Molded rigid polymer monoliths as separation media for capillary electrochromatography. Anal Chem 69(17):3646–3649
30. Yang M, Yang Y, Liu Y, Shen G, Yu R (2006) Platinum nanoparticles-doped sol–gel/carbon nanotubes composite electrochemical sensors and biosensors. Biosens Bioelectron 21 (7):1125–1131
31. Hilder EF, Svec F, Fréchet JMJ (1997) Latex-functionalized monolithic columns for the separation of carbohydrates by micro anion-exchange chromatography. J Chromatogr A 1053(1–2):101–106
32. Yang WT, Rånby B (1996) Bulk surface photografting process and its applications. 1. Reactions and kinetics. J Appl Polymer Sci 62 (3):533–543
33. Yang WT, Rånby B (1996) Bulk surface photografting process and its applications. 2. Principal factors affecting surface photografting. J Appl Polymer Sci 62(3):545–555
34. Stachowiak TB, Svec F, Fréchet JMJ (2006) Patternable protein resistant surfaces for multifunctional microfluidic devices via surface hydrophilization of porous polymer monoliths using photografting. Chem Mater 18(25):5950–5957
35. Gillespie E, Connolly D, Paull B (2009) Using scanning contactless conductivity to optimise photografting procedures and capacity in the production of polymer ion-exchange monoliths. Analyst 134(7):1314–1321
36. Connolly D, Floris P, Nesterenko PN, Paull B (2010) Non-invasive characterization of stationary phases in capillary flow systems using scanning capacitively coupled contactless conductivity detection (sC^4D). Trends Anal Chem 29(8):870–884
37. Chatenet M, Micoud F, Roche I, Chainet E (2006) Kinetics of sodium borohydride direct oxidation and oxygen reduction in sodium hydroxide electrolyte: Part I. BH_4^- electro-oxidation on Au and Ag catalysts. Electrochim Acta 51(25):5459–5467
38. Henglein A, Lilie J (1981) Radiation electrochemistry of the colloidal cadmium microelectrode. Catalysis of hydrogen formation by organic free-radicals. J Phys Chem 85(9):1246–1251
39. Henglein A, Lilie J (1981) Storage of electrons in aqueous solution: the rates of chemical charging and discharging the colloidal silver microelectrode. J Am Chem Soc 103(5):1059–1066
40. Freund T (1959) Kinetics of the reduction of inorganic ions by borohydride: 1 Ferricyanide. J Inorg Nucl Chem 9(3–4):246–251